Water desalination by silica supported ionic liquid

Water desalination by silica supported ionic liquid: adsorption kinetics and system modeling

Ahmed A. Askalany[a,*], Kutub Uddin[b,c], Bidyut B. Saha[b,d], Muhammad Sultan[e], Giulio Santori[f]

[a] Mechanical Engineering, Faculty of Technology and Education, Sohag University, Sohag 82524, Egypt

[b] International Institute for Carbon-Neutral Energy Research, Kyushu University, 744 Motooka, Nishi-ku, Fukuoka 819-0395, Japan

[c] Faculty of Physics, Jagannath University, Dhaka 1100, Bangladesh

[d] Mechanical Engineering Department, Kyushu University, 744 Motooka, Nishi-ku, Fukuoka 819-0395, Japan

[e] Department of Agricultural Engineering, Bahauddin Zakariya University, Bosan Road, Multan 60800, Pakistan

[f] The University of Edinburgh, School of Engineering, Institute for Materials and Processes, Sanderson Building, The King's Buildings, Mayfield Road, EH9 3BF Edinburgh, Scotland, UK

*Corresponding Author, Tel: +201028721274

E-mail: ahmed_askalany3@yahoo.com

Abstract

Significant efforts have been done in order to improve adsorption desalination systems by developing advanced adsorbents. Silica-supported ionic liquid (SIL) has been recently proposed as a promising adsorption material for water desalination due to its relatively high adsorption capacity around 1 $kg_{water}.kg_{SIL}^{-1}$. Such achieved performance can be considered as an initial cornerstone that requires further important additional data before reaching a successful practical application. In this paper, experimental measurements of water adsorption kinetics in the SIL named EMIM-AC/Syloid 72FP are presented. The kinetics is interpreted using a linear driving force (LDF) model that shows good harmony with experimental data. Depending on a former study on adsorption isotherms and the current kinetics data, the performance of an adsorption water

desalination system (ADS) is predicted using a dynamic lumped parameter model. The results show a bright future for this SIL material in water desalination application with high theoretical pure water production achieving 47 m^3 $day^{-1}ton^{-1}$, 0.85 coefficient of performance with 600 W kg_{SIL}^{-1} specific cooling power. Furthermore, system working with the EMIM-AC/Syloid 72FP can theoretically be powered by as low as 40°C heat source.

Keywords: Adsorption; kinetics; desalination; silica gel; ionic liquid

Nomenclature

Symbols		
A	Area	m^2
C	Adsorption capacity	kg kg^{-1}
C_o	Maximum adsorption capacity	kg kg^{-1}
C_p	Specific heat	$J.kg^{-1}.K^{-1}$
D_s	Surface diffusion coefficient	$m^2.s^{-1}$
D_{so}	Pre-exponential coefficient	$m^2.s^{-1}$
E	Characteristic energy	$J.mol^{-1}$
E_a	Activation energy	$J.mol^{-1}$
h_{fg}	Water latent heat	$J.kg^{-1}$
H_{st}	Adsorption heat	$J.kg^{-1}$
M	Mass	kg
m .	Mass flow rate	$kg.s^{-1}$
n	Dubinin-Astakhov fitting parameter	
P	Pressure	kPa
R	Gas constant	$J.mol^{-1}.K^{-1}$
R_p	Average particle radius	m
T	Temperature	°C
X	Concentration	ppm
t	Time	S

W_0	Saturation uptake	$cm^3.g^{-1}$

Subscripts/Superscript

ads	Adsorption
al	Aluminum
b	Brine
bed	Adsorption bed
cond	Condenser
ch	Chilled water
cu	Copper
des	Desorption
evap	Evaporator
hex	Heat exchanger
hw	Heating water
i	Inlet
o	Outlet
s	Salt
sat	Saturation
sg	Silica gel
sw	Seawater
v	Vapor
w	Water

1. Introduction

Adsorption technology applications, especially in heat transformation, drying, and water purification, are getting attention thanks to the promising features for a zero-emissions future. These systems are still at research and development stage to solve issues such as low efficiency and productivity. Nevertheless, adsorption technologies still remain a strong antagonist to traditional electricity-driven technologies as they are environment-friendly due to their ability to be driven by clean energy and operate with clean fluids.

The research efforts are currently spent at material development, components, and system levels to produce highly efficient and reliable adsorption devices for heat transformation, drying, and water purification. The primary focus here is to assess high-performance adsorption desalination systems (ADSs) employing a newly synthesized material. In principle, we found that the same material is suitable for drying and cooling.

Research avenues include materials for ADSs that have high adsorption uptake, components with improved heat and mass transfer, and at a system level, the integration of ADS with other water purification systems. In 1984, Broughton presented the first AD cycle using anion-retarded resin as adsorbent [1]. Further developments later were conducted to raise the efficiency of the ADSs. Wang and Ng presented four-bed ADS employing silica gel/water [2]. This plant provided specific daily water production (SDWP) of 4.7 $kg.kg_{sg}^{-1}$ at 85°C, 29.4°C, and 12.2°C for beds, condenser, and evaporator, respectively [2]. El-Sharkawy et al. also reported that the ADS could produce an SDWP of 8.2 $kg.kg_{sg}^{-1}$ at an ambient temperature of the chilled water [3].

A laboratory-scale two-beds solar-powered ADS was investigated by Ng et al. using a 215 m^2 solar collector achieving an SDWP up to 5 $kg.kg_{sg}^{-1}$ [4]. Thu et al. presented an idea of heat recovery between the evaporator and the condenser of ADS showing an increase in the SDWP up to 9.34 $kg.kg_{sg}^{-1}.day^{-1}$ at a heating temperature of 70°C [5]. ADS and the cooling pilot plant were built containing four silica gel-packed beds and driven by flat-plate solar collectors with an area of 485 m^2 [6]. The plant produced an SDWP of 12.5 $kg.kg_{sg}^{-1}$ and 84 kW cooling capacity at 85°C, 30°C, and 7°C regeneration temperature, cooling, and chilled water, respectively. Later, this plant was analyzed theoretically by Thu et al., assuming internal heat recovery showing that the plant could duplicate the SDWP at the same regeneration temperature [7].

A zeolite-based material, AQSOA-Z02, was proposed to be employed in ADSs [8,9]. At 10°C evaporator water temperature, the AQSOAZ02 cycle produced an SDWP and specific cooling power (SCP) of 5.8 $kg_{water}.kg_{zeolite}^{-1}$ and 176 kW, respectively [8]. With 4-beds ADS employing AQSOA-Z02, Youssef et al. conducted a numerical study that achieved an SDWP of 12.4 $kg_{water}.kg_{zeolite}^{-1}$ with an SCP of 114 $W.kg_{zeolite}^{-1}$ at an evaporator water temperature of 10°C utilizing heat recovery between system components [10].

Askalany et al. proposed theoretically an innovative combination of mechanical vapor compression (MVC) and ADS achieving an SDWP and SCP of 14 $kg_{water}.kg_{silica\ gel}^{-1}$ and 0.21

$kW.kg_{silica\ gel}^{-1}$ respectively [11]. Alsaman et al. built a solar-powered ADS under Egypt's climate conditions using 4.5 m^2 solar collector (evacuated tube) where an SDWP of 5.3 $kg_{water}.kg_{silica\ gel}^{-1}$ was produced using a cooling temperature of 25°C. SDWP of 8 $kg_{water}.kg_{silica\ gel}^{-1}$ was stated at 15°C cooling water temperature [12]. Thu et al. investigated multi-bed adsorption with heat recovery producing an SDWP of 10 $kg_{water}.kg_{silica\ gel}^{-1}$ at a driving temperature of 70°C [13].

CPO-27(Ni) Metal-organic frameworks (MOFs), was employed in a 1-bed adsorption system. An SDWP of 22.8 $kg_{water}.kg_{MOF}^{-1}$ was achieved using 40°C evaporator temperature, 5°C condenser temperature, and 95°C desorption temperature [14].

3-stages Multi-effect desalination (MED) integrated with 4-beds ADS was studied. The hybrid MEDAD achieved up to 2.5 to 3 folds an increase in the produced distilled water than a MED. Later, it was stated that the MEAD cycle with 7 intermediate stages produced an SDWP of 24 $kg_{water}.kg_{silica\ gel}^{-1}$ [15–17].

Thus, great efforts have been spent on improving the performance of the ADSs at system levels and only a few investigations have focused on material development and characterization. All the investigations above propose solutions to increase the technology performance and ideally pave the way to its commercial deployment. Unfortunately the performance achieved so far have been promising but not high enough for practical utilization. Recently, a new adsorption material, silica-supported ionic liquid (SIL) EMIM-AC/Syloid 72FP, has been developed, showing promising features for application in adsorption heat transformation [18,19]. This material stands out in terms of thermodynamic properties, with extremely low regeneration temperatures required (<50°C) and heat of adsorption coincident with the latent heat of water in a large range of water uptakes.

The previous study on this material showed its preparation and adsorption isotherms [19]. To use the material in water desalination devices the knowledge of its adsorption characteristics (isotherms and kinetics) is essential, along with modeling the device performance by using the material data in order to have practical design guidelines [20–22]. System modeling is a necessary step before building any system to save trial and error efforts, time, and money. Up to now, only the preparation and the adsorption isotherms were presented, which leads to a gap in adsorption kinetics that should be filled. Accordingly, the characterization of the new material is completed with kinetic measurements of water sorption onto EMIM-AC/Syloid 72FP. Additionally, a model for an ADS employing the SIL EMIM-AC/Syloid 72FP is studied to assess the system-level

performance. The presented data are the essential complement to the equilibrium data and can help any researcher in this field willing to employ this material.

2. Adsorption kinetics

2.1.Test rig and experimental procedures

The adsorption measurement unit consists mainly of a suspended magnetic balance that weighs masses with no direct contact between the measuring mass and the weighing tool [23]. Fig. 1 shows a diagram for the magnetic suspension adsorption measuring unit. Water adsorption characteristics onto the SIL EMIM-AC/Syloid material are measured within the adsorption temperature range 30 to 70°C. A multi-step adsorption technique is used in each experiment where the adsorption temperature is constant while evaporator temperature increases step by step until reaching a P/P_s of about 0.9 or above. The equilibrium condition is ensured at each evaporation temperature.

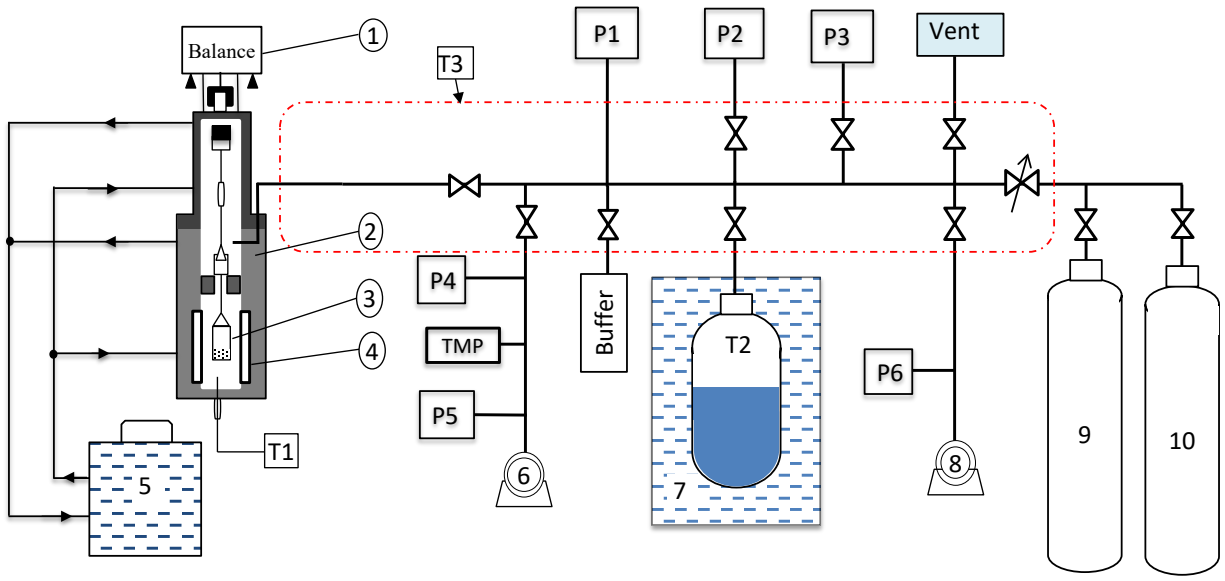

Fig. 1. Schematic of a test rig for adsorption equilibrium and kinetic measurements.

1. Magnetic suspension balance for measuring the weight of the sample, 2. Circulation oil jacket 3. Sample basket, 4. Sheathed heater, 5 & 7. Isotherm oil bath, 6 & 8. Rotary and diaphragm pump, 9&10. Nitrogen and Helium cylinder, T1-T3: Thermocouple, P1-P6: Pressure gauge, TMP: Turbomolecular pump.

For each isotherm measurement, the following steps are taken;

I. About 60 mg of dry adsorbent sample is placed in the basked (3).

II. The sorbent sample is regenerated at 90°C for about 4 hours in a vacuum condition to remove if there are any adsorbed impurities in the sample. This turbomolecular (TMP) pump can provide down to 3×10^{-5} Pa vacuum during regeneration. After that, the sample is cooled down to the adsorption temperature (T1) and measured the dry sample weight.

III. The buoyancy effect of the measurement is considered automatically using helium gas and measuring the sample weight again.

IV. The valves between the adsorption cell and water vapor are opened when the sample cell and water vapor reach the setting temperature condition. Then adsorption process starts, and the adsorbed amount is continuously recorded using the magnetic suspension balance. The process continues until reaching the equilibrium conditions corresponding to the setting first evaporation temperature (T2).

V. After reaching the first equilibrium condition, the valve between the evaporator and adsorption chamber is closed, and the evaporator starts to increase the temperature to prepare for the next relative pressure step. Process (iv) and (v) are repeated for second, third, and other relative pressure.

The piping system is always kept at a temperature 10 ºC higher than the adsorption temperature to avoid condensation, which was reached by the isotherm air bath surrounding the piping system (T3). The valves are operated automatically using N_2 gas following the provided setting condition. Platinum thermocouples and absolute pressure gauges are used in measuring temperatures and pressure, respectively.

In this thermogravimetric apparatus, the weight of the sample is estimated by a resolution of 1 μg for measuring scale around 10g, and the reproducibility (standard deviations) is ±1μg when the sample mass is about 5g. The sample mass used ranged between 60 and 65 mg. the relative error on the water uptake is always less than 0.001%.

2.2.Results

Linear Driving Force (LDF) is a popular model for analyzing gas adsorption kinetics thanks to its physically consistent, analytic, and simple features. LDF parameters can be retrieved from (a) the evaluation of the uptake on a heterogeneous porous material, (b) the calculation of breakthrough

curves in a packed adsorbent column, and (c) the efficiency of separation in an adsorptive process by repeated averaging of the base kinetic property [24].

To estimate parameters of LDF [25,26], Arrhenius plot is presented in Fig. 2, showing heat-dependent kinetic parameters on Eq. 2 and Eq. 3. Based on the estimated parameters of the Arrhenius plot (pre-exponential coefficient and Activation energy), LDF is fitted against the measured adsorption capacity of EMIM-AC/Syloid 72FP for different temperatures (20 ^{o}C – 60 ^{o}C in Fig. 3), showing good agreement at different temperatures. Extracted parameters from the Arrhenius plot are shown in Table. 1.

$$\frac{dC}{dt} = k_s a_v (C_o - C) \tag{1}$$

$$k_s a_v = F_o \frac{D_s}{{R_p}^2} \tag{2}$$

$$D_s = D_{so} \exp\left(-\frac{E_a}{RT}\right) \tag{3}$$

where D_s ($m^2.s^{-1}$) is a surface diffusion coefficient, D_{so} ($m^2 .s^{-1}$) is a pre-exponential coefficient and E_a ($J.mol^{-1}$) is an activation energy.

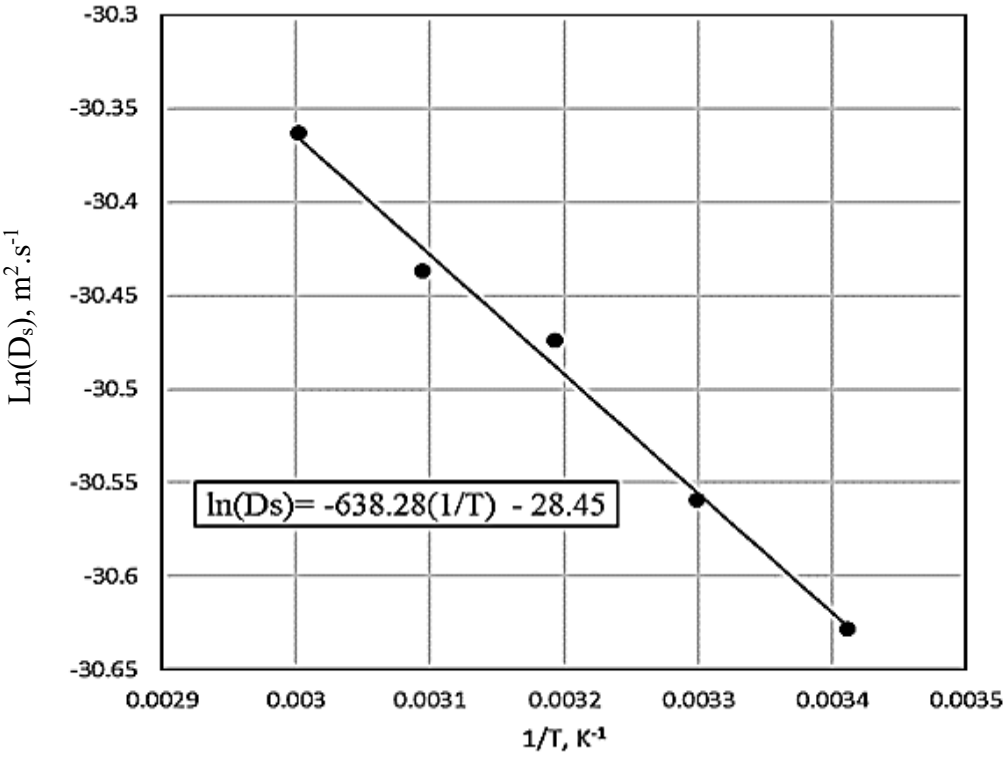

Fig. 2. Arrhenius plot of the water/EMIM-AC/Syloid 72FP pair.

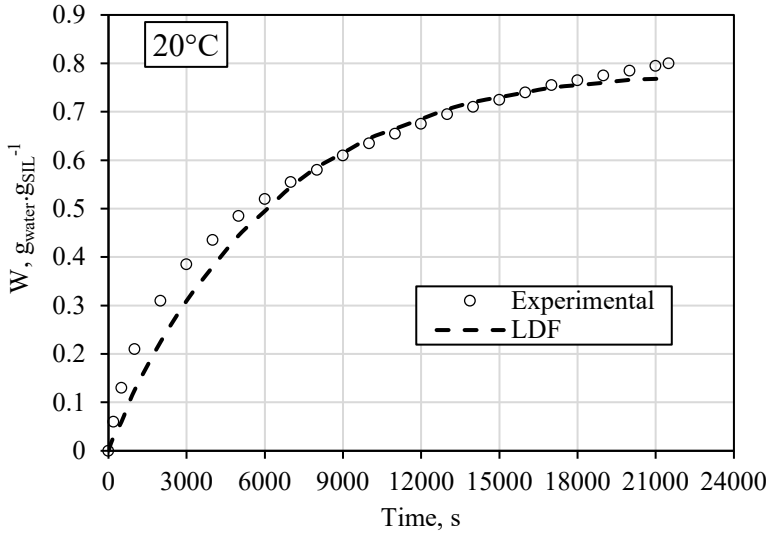

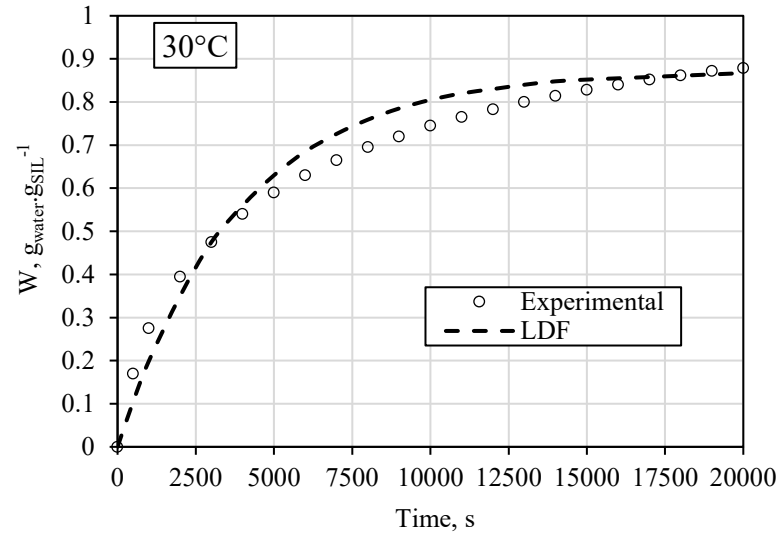
30°C
W, $g_{water}.g_{SIL}^{-1}$
Experimental
LDF
Time, s

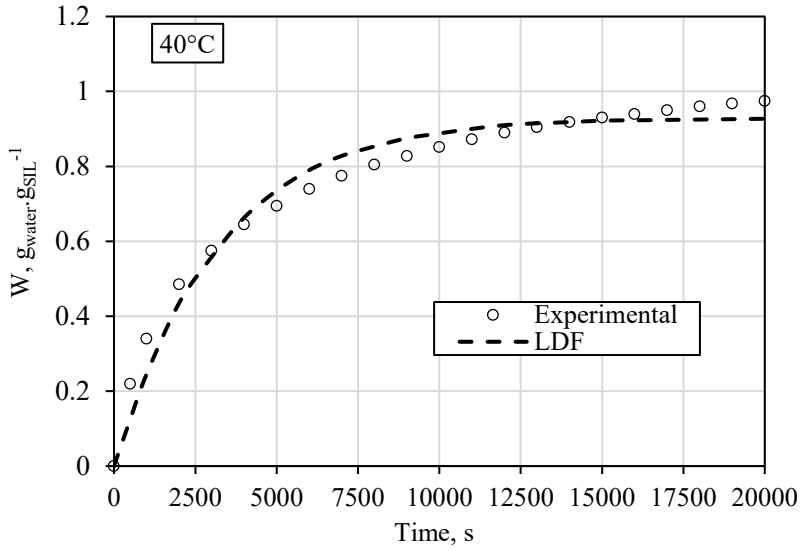
40°C
W, $g_{water}.g_{SIL}^{-1}$
Experimental
LDF
Time, s

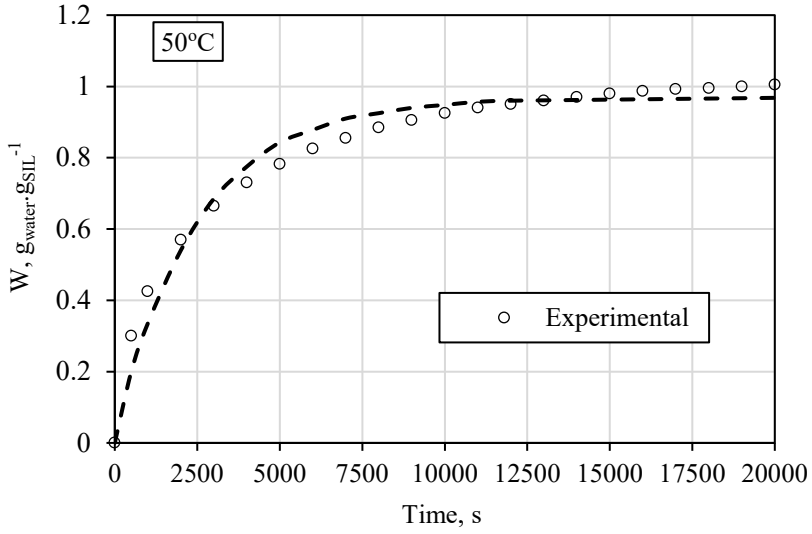
50°C
W, $g_{water}.g_{SIL}^{-1}$
Experimental
Time, s

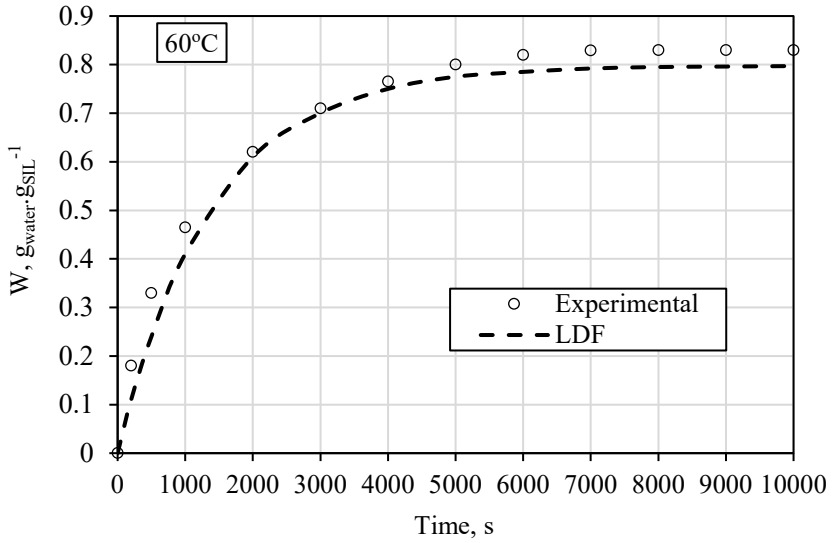

Fig. 3. LDF fitting of experimental uptake of EMIM-AC/Syloid 72FP at different temperatures (20°C, 30°C, 40°C, 50°C, and 60°C).

Table 1. Parameters of the LDF for EMIM-AC/Syloid 72FP-water pair.

Parameter	Value
D_{s0} (pre-exponential coefficient), $m^2.s^{-1}$	$4.41\ 10^{-13}$
E_a (activation energy), $kJ.kmole^{-1}$	5306.66

3. Theoretical model

3.1.System description

In order to test the potential of SIL for adsorption desalination and/or cooling applications, a theoretical investigation from experimental equilibrium and non-equilibrium parameters is the initial and essential step before any experimentation at the system level. Therefore, a theoretical adsorption desalination/cooling model is developed. The model simulates the system reported in Fig. 4, which includes two adsorption beds, condenser, and evaporator. Two beds type has been chosen for presenting a semi-continuous cooling effect.

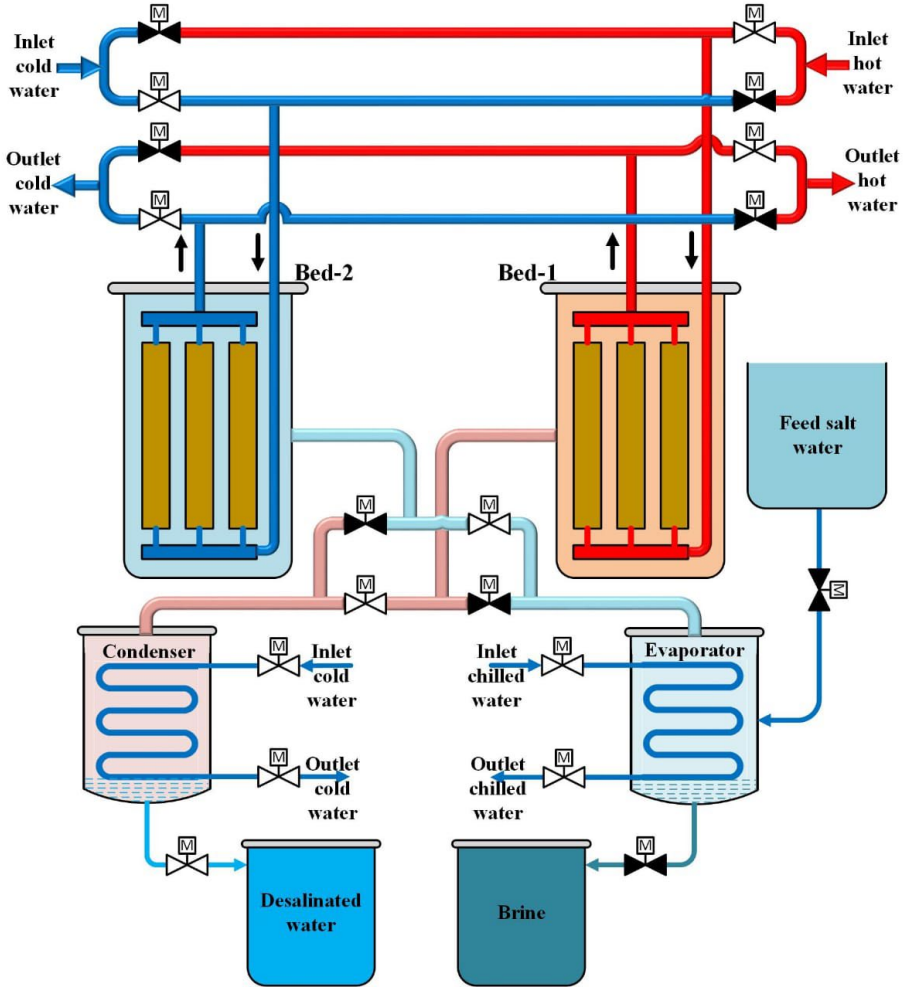

Fig. 4. Two beds adsorption desalination/cooling system.

3.2.Mathematical model

Equations that simulate the ADS in the form of adsorption equilibrium and kinetics of the adsorption pair are presented in the next section. Mass and energy balances of the condenser, evaporator, and adsorption bed are also presented in the following section.

Equilibrium water uptake

D-A model for water adsorption onto silica gel, adsorption isotherms [27-29]

$$C = C_{\circ} exp\left\{-\left(\frac{RT}{E} ln\left(\frac{P_{sat}}{P}\right)\right)^{n}\right\} \quad (4)$$

Mass balance equations for saltwater and condensate water mass balance

$$\frac{dM_{sw,evap}}{dt} = \dot{m}_{sw,in} - \dot{m}_{p,cond} - \dot{m}_b \tag{5}$$

Evaporator and salt mass balance

$$\frac{dM_{sw,evap}}{dt} = \dot{m}_{sw,in} - \dot{m}_b - \left(\frac{d_{Cads}}{dt}\right) M_{ads} \tag{6}$$

$$M_{sw,eva}\frac{dX_{sw,evap}}{dt} = X_{sw,in}\dot{m}_{sw,in} - X_{sw,in}\dot{m}_b - X_D\left(\frac{d_{Cads}}{dt}\right) M_{ads} \tag{7}$$

Energy balance equations employed for adsorption beds

$$\left[(Mc_p)_{cu} + (Mc_p)_{al} + (Mc_p)_{ads} + M_{ads}c_{p_v}C\right]^{bed}\frac{dT_{bed}}{dt} = M_{ads}H_{st}\frac{\mathrm{dC}}{dt} - \dot{m}_w c_{p_w}(T_{w,out} - T_{w,in}) \tag{8}$$

Heat of adsorption

$$H_{st} = h_{fg} + E\left[ln\left(\frac{C_o}{C}\right)^{\frac{1}{n}}\right] + \frac{ET\alpha}{n}\left[ln\left(\frac{C_o}{C}\right)\right]^{\frac{1-n}{n}} \tag{9}$$

Condenser energy balance

$$\left[(Mc_p)_{cu} + (Mc_p)_{iron} + (Mc_p)_w\right]\frac{dT_{cond}}{dt} = h_f(T_{cond})\frac{dM}{dt} + h_{fg}(T_{cond})\frac{dC_{des}}{dt}M_{ads} + \dot{m}_w c_{p_w}(T_{cond})\left(T_{w,in} - T_{w,out}\right)^{cond}\dot{m}_b \tag{10}$$

Evaporator energy balance

$$\left[M_{s,evap}c_{p_s}(T_{evap}, X_{s,evap}) + M_{cu,evap}c_{p_{cu,evap}}\right]\frac{dT_{eva}}{dt} = h_f(T_{evap}, X_{s,evap})\dot{m}_{s,in} - h_{fg}(T_{evap})\frac{dC_{des}}{dt}M_{sg} + \dot{m}_{ch}c_{p_{ch}}(T_{ch,in} - T_{ch,out}) - h_f(T_{evap}, X_{s,evap})\dot{m}_b \tag{11}$$

Temperature of the outlet water of the heat exchanger is expressed as;

$$T_{w,out} = T_{hex} + (T_{w,in} - T_{hex})exp\left(\frac{-UA_{hex}}{(\dot{m}c_p)_w}\right) \tag{12}$$

Cooling load, desorption, and condensation energy are given by;

$$Q_{eva} = \int_0^{t_{cycle}} \dot{m}_{ch}c_{p_{ch}}(T_{ch,in} - T_{ch,out})dt \tag{13}$$

$$Q_{des} = \int_0^{t_{cycle}} \dot{m}_{hw} c_{p_w} \left(T_{hw,in} - T_{hw,out}\right) dt \quad (14)$$

$$Q_{cond} = \int_0^{t_{cycle}} \dot{m}_{w} c_{p_w} \left(T_{cw,in} - T_{cw,out}\right) dt \quad (15)$$

Cycle performance parameters

$$SDWP = \frac{24 * 60 * 60}{t_{cycle}} \int_0^{t_{cycle}} \frac{\dot{m}_{w} c_{p_w} \left(T_{cw,out} - T_{cw,in}\right)}{h_{fg} M_{sg}} dt \quad (16)$$

$$SCP = \int_0^{t_{cycle}} \frac{\dot{m}_{ch} c_{p_{ch}} \left(T_{ch,in} - T_{ch,out}\right)}{M_{sg}} dt \quad (17)$$

Coefficient of performance (COP)

$$COP = \int_0^{t_{cycle}} \frac{\dot{m}_{ch} c_{p_{ch}} \left(T_{ch,in} - T_{ch,out}\right)}{\dot{m}_{hw} c_{p_w} \left(T_{hw,in} - T_{hw,out}\right)} dt \quad (18)$$

Differential algebraic system of equations is solved in FORTRAN. The used parameters are indicated in Table 2 [30].

Table 2. Model parameters.

Parameters	Description	Value	Unit
UA_{bed}	Overall heat transfer coefficient of bed	600	$W.K^{-1}$
UA_{cond}	Overall heat transfer coefficient of condenser	500	$W.K^{-1}$
UA_{eva}	Overall heat transfer coefficient of evaporator	350	$W.K^{-1}$
M_{cu}	Bed heat exchangers tube weight (Cu)	2.97	kg
M_{al}	Bed heat exchanger fin weight (Al)	0.72	kg
$M_{bed,iron}$	Bed heat exchanger cover weight (Iron)	15	kg
$M_{cond,cu}$	Condenser heat exchangers tube weight (Cu)	1.535	kg
$M_{eva,cu}$	Evaporator heat exchangers tube weight (Cu)	1.3	kg
$M_{w,eva}$	Liquid water inside evaporator initially	1	kg
M_{ads}	Weight of adsorbent in each bed	6.75	kg
$\dot{m}_{hw}$	Heating water flow rate to the adsorber	0.2	kg/s
$\dot{m}_{chw}$	Chilled water flow rate	0.025	kg/s
$\dot{m}_{cw}$	Cooling water flow rate to the adsorber	0.3	kg/s
W_0	Saturation uptake	38.78	$cm^3.g^{-1}$ [31]
E	Characteristic energy	12.8	$J.mol^{-1}$ [31]
n	Dubinin-Astakhov fitting parameter	0.27	[31]
Cp_{cu}	Copper specific heat	0.386	J/kg.K
Cp_{al}	Aluminum specific heat	0.905	J/kg.K
Cp_{ads}	Adsorbent specific heat	0.924	J/kg.K
Cp_{w}	Water specific heat in liquid phase	4.18	J/kg.K
Cp_{ch}	Chilled water specific energy in the vapor phase	4.20	J/kg.K
Cp_{v}	Water specific heat in vapor phase	1.89	J/kg.K
R	Universal gas constant	8.314	J/kg.K
R_p	Average radius of adsorbent particle	0.0058	mm [32]
T_{hw}	Heating source temperature	95-75	°C
T_{cw}	Cooling source temperature	30	°C
$T_{ch,in}$	Chilled water inlet temperature	30	°C
t_{cycle}	Cycle time	650	Sec

4. Results and discussion

A desalination system employing EMIM-AC/Syloid 72FP has been modeled. The effect of the main controllable parameters such as regeneration and evaporator temperatures on the Specific Daily Water Production (SDWP), Specific Cooling Power (SCP) and Coefficient of Performance (COP) is studied to optimize the system operation.

Effect of regeneration temperatures (from 313.15 K to 363.15 K) and evaporator temperatures (from 280 K to 297.15 K) on the SDWP is shown in Fig. 5. The SDWP can achieve up to 47 m^3day^{-1} ton_{water}^{-1}. The increase of regeneration and evaporator temperatures has a good impact on the SDWP in around 333.15 K and 297.5 K regeneration and evaporator temperatures, respectively. No water is gained in the region of evaporator temperatures less than 285.15 K and regeneration temperature less than 333.15 K. Therefore, a falling off in the evaporator temperature and accordingly in the evaporator pressure leads to a contraction in the initial capacity of the cycle resulting in a decrease in produced water vapor.

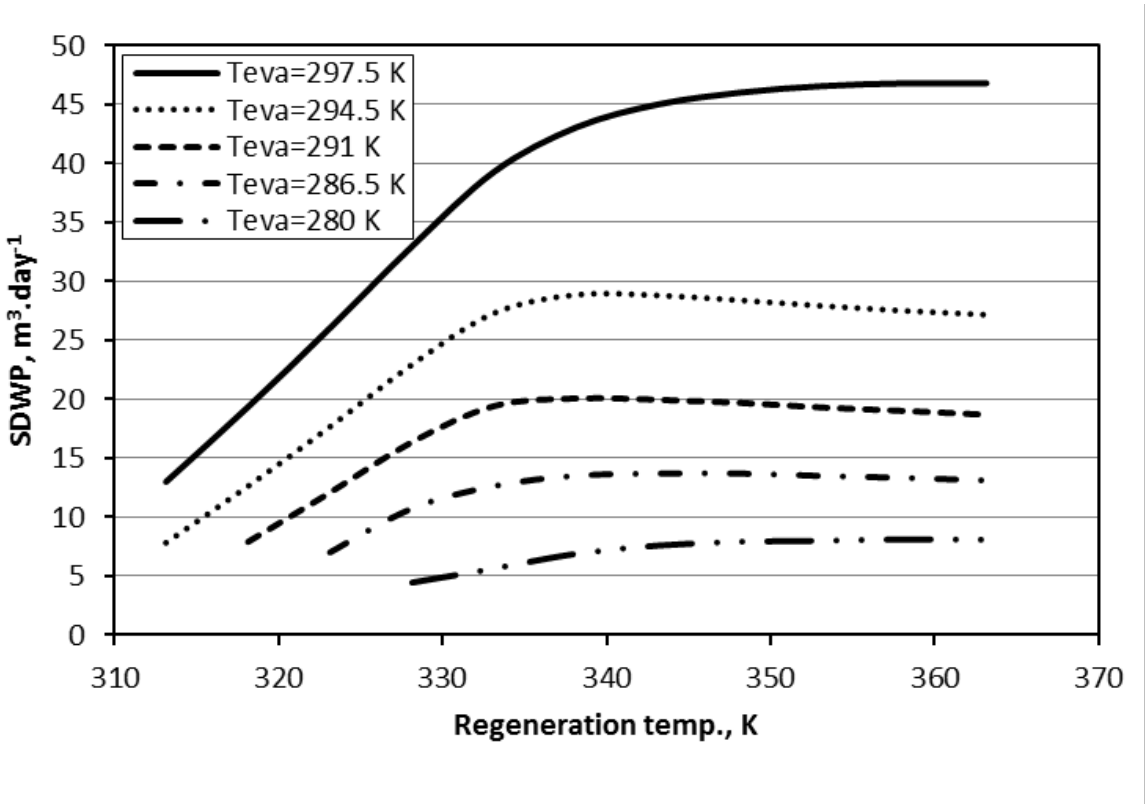

Fig. 5. Effect of regeneration and evaporator temperatures on SDWP of EMIM-AC/Syloid 72FP at 30°C condenser temperature.

Cycle time effect in the range from 500 s to 4500 s at different heating temperatures on the SDWP is presented in Fig. 6 for 297.5 K evaporator temperature. Overall, the decrease of cycle time has a good impact on the SDWP, where a relatively fast cycle of 500 s with 363.15 K regeneration temperature achieved the highest SDWP of 67 $m^3.day^{-1}.ton^{-1}$. Large cycle times have a negative impact on the SDWP. Fig. 6 also shows that the cycle time has a greater effect on SDWP than the heating temperature.

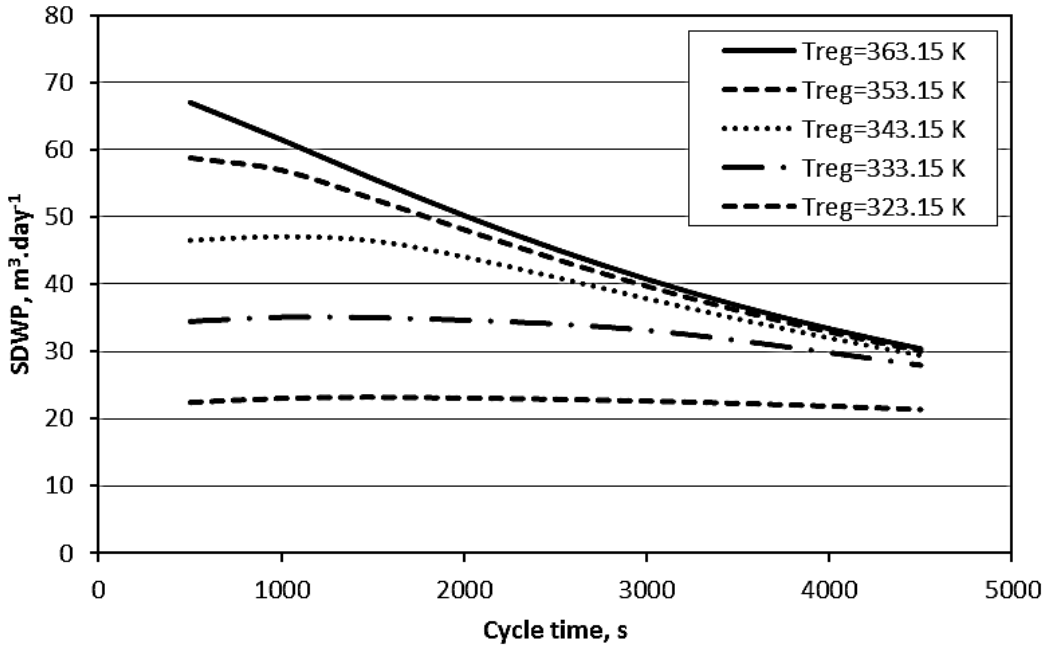

Fig. 6. Cycle time dependent SDWP of EMIM-AC/Syloid 72FP at different regeneration temperatures (297.5 K evaporator temperature) at 30°C condenser temperature.

SCP at different heating temperatures in the range of 313.15-363.15 K and evaporator temperatures of 280 up to 294.5 K are presented in Fig. 7. Generally, raising the evaporator temperature produces a rise in the SCP. That is because the increase of the evaporator temperature causes a rise in the starting pressure of the cycle, which raises also the cycle's initial capacity. Accordingly, the desorbed amount of vapor increases. Also, the increase of the heating temperature to 340 K has a good impact on the SCP, while any further increase does not effect on SCP. Therefore, from the

cooling point of view, the optimum conditions are 340 K heating temperature and 294.5 K evaporator temperature.

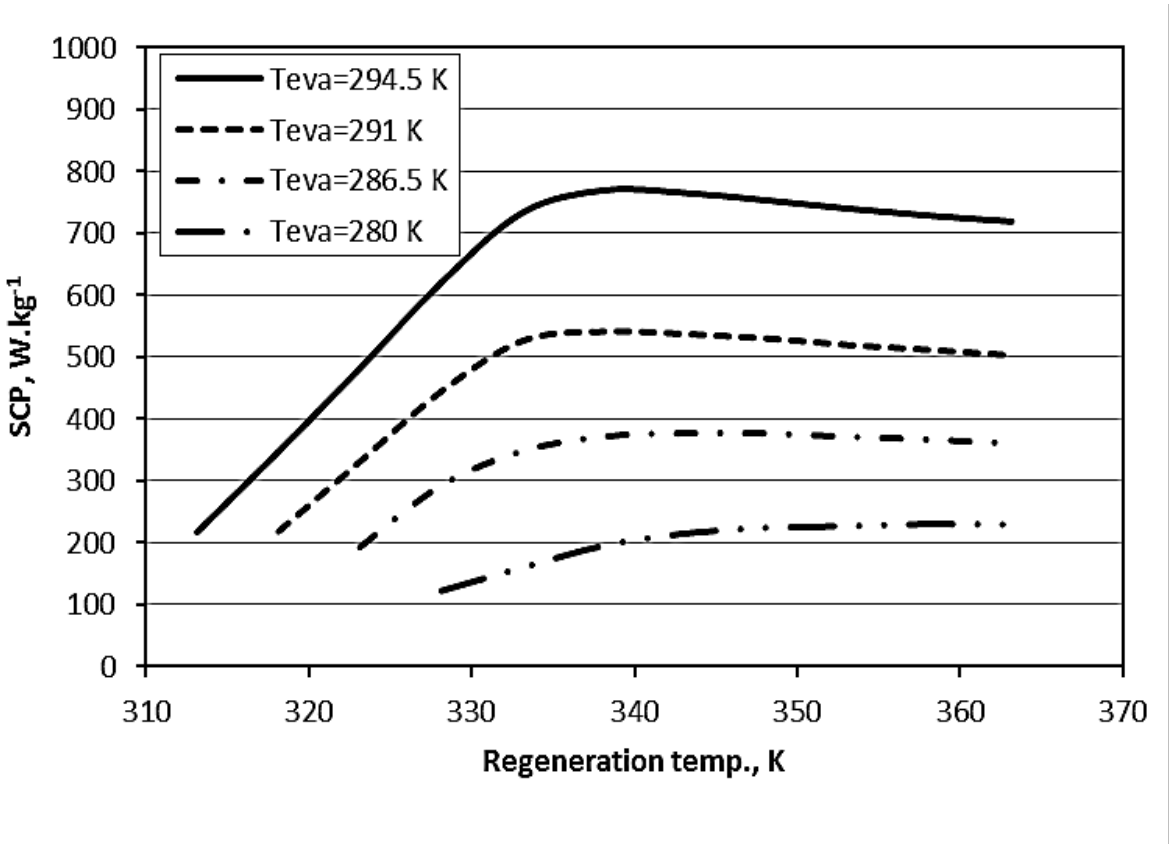

Fig. 7. SCP of EMIM-AC/Syloid 72FP system for different heating and evaporator temperatures at 30 °C condenser temperature.

The COP can achieve values as high as 0.9 at a heating temperature of 313.15 K and evaporating temperature of 294.5 K. At a lower evaporating temperature of 286 K, the COP reduces to 0.78 can be . Unlike the SCP and SDWP, the regeneration temperature has a bad effect on the COP for temperatures higher than 340 K. Where raising the bed temperature leads to an increase in temperatures of the associated metal parts such as the tubes, fins, and outer casing of the bed resulting in an increase of cycle time, without any increase of the working capacity.

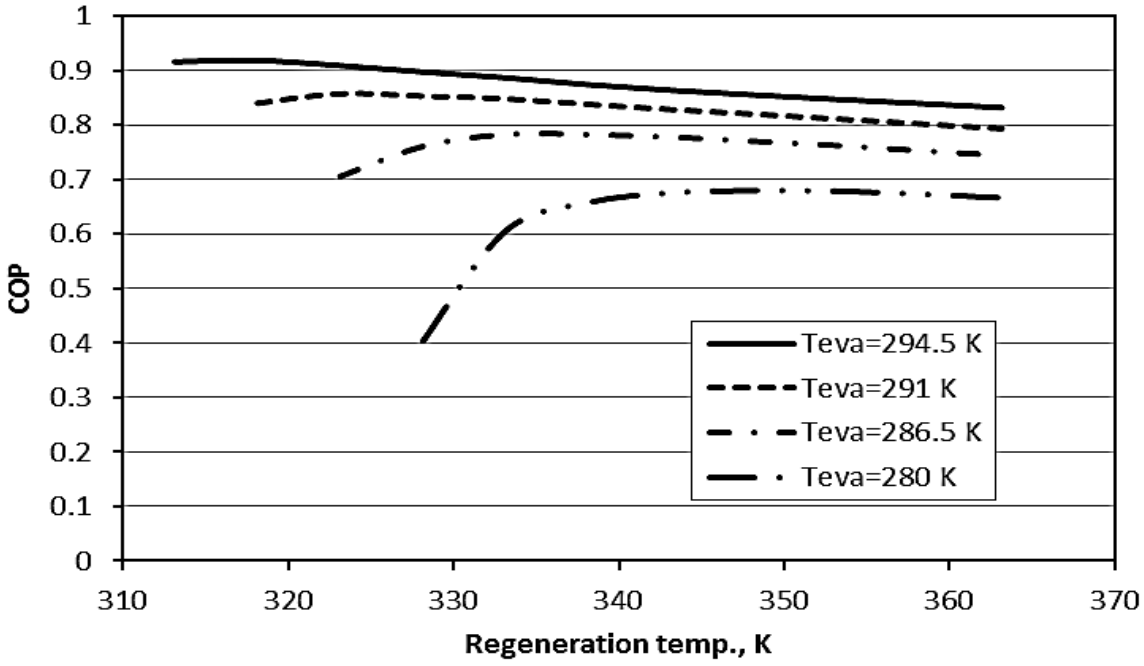

Fig. 8. COP of EMIM-AC/Syloid 72FP system for different heating and evaporator temperatures.

5. Conclusions

This work complements a series of investigations focusing on SIL materials as a new adsorbent materials for water desalination applications with a high relatively adsorption capapcity. This started by measuring the isotherms on the investigated material [19]. As second step, this investigation has focused on measuring the water adsorption kinetics of the material and modelling the operation of a complete system.

The kinetics of the supported ionic liquid composite material EMIM-AC/Syloid 72FP has been measured and the data have been regressed by using the linear driving force model, providing a value for the linear driving force constant. The utilization of the material in cooling and desalination has been assessed theoretically on the basis of the experimental data from the kinetic measurements.

Results proved that the SDWP could achieve values up to 47 $m^3.day^{-1}$ per ton of EMIM-AC/Syloid 72FP. It is shown that cycle times as short as 500s have a beneficial effect on the SDWP and on

the SCP of the cycle. A relatively fast cycle of 500 s with 60°C regeneration temperature showed the highest SDWP. SCP higher than 400 $W.kg_{SIL}^{-1}$ could be achieved at a relatively low regeneration temperature of 60°C and 9°C evaporator temperature. This system can be driven using a low heat source temperature at 40°C. According to the shown results, the EMIM-AC/Syloid 72FP adsorbent can double the current achievements in water productivity by using heat at extremely low driving temperatures.

Acknowledgments

The research leading to these results has received funding from the EPSRC "Micro-scale energy storage for super-efficient wet appliances" project EP/P010954/1.

References

[1] Broughton DB. Continuous desalination process 1984.

[2] Wang X, Ng KC. Experimental investigation of an adsorption desalination plant using low-temperature waste heat. Appl Therm Eng 2005;25:2780–9. https://doi.org/10.1016/j.applthermaleng.2005.02.011.

[3] El-Sharkawy II, Thu K, Ng KC, Saha BB, Chakraborty A, Koyama S. Performance improvement of adsorption desalination plant: experimental investigation. Int Rev Mech Eng 2007;1:25–31.

[4] Ng KC, Thu K, Chakraborty A, Saha BB, Chun WG. Solar-assisted dual-effect adsorption cycle for the production of cooling effect and potable water. Int J Low-Carbon Technol 2009;4:61–7.

[5] Thu K, Saha BB, Chakraborty A, Chun WG, Ng KC. Study on an advanced adsorption desalination cycle with evaporator-condenser heat recovery circuit. Int J Heat Mass Transf 2011. https://doi.org/10.1016/j.ijheatmasstransfer.2010.09.065.

[6] Ng KC, Thu K, Kim Y, Chakraborty A, Amy G. Adsorption desalination: An emerging low-cost thermal desalination method. Desalination 2013;308:161–79. https://doi.org/10.1016/j.desal.2012.07.030.

[7] Thu K, Yanagi H, Saha BB, Ng KC. Performance analysis of a low-temperature waste heat-driven adsorption desalination prototype. Int J Heat Mass Transf 2013;65:662–9.

https://doi.org/10.1016/j.ijheatmasstransfer.2013.06.053.

[8] Charalambous C, Santori G, Vilarrasa-Garcia E, Bastos-Neto M, Cavalcante Jr CL, Brandani S. Pure and binary adsorption of carbon dioxide and nitrogen on AQSOA FAM Z02. J Chem Eng Data 2018;63:661–70.

[9] Youssef PG, Mahmoud SM, AL-Dadah RK. Performance analysis of four bed adsorption water desalination/refrigeration system, comparison of AQSOA-Z02 to silica-gel. Desalination 2015;375:100–7. https://doi.org/10.1016/j.desal.2015.08.002.

[10] Youssef PG, Mahmoud SM, AL-Dadah RK. Numerical simulation of combined adsorption desalination and cooling cycles with integrated evaporator/condenser. Desalination 2016;392:14–24. https://doi.org/10.1016/j.desal.2016.04.011.

[11] Askalany AA. Innovative mechanical vapor compression adsorption desalination (MVC-AD) system. Appl Therm Eng 2016;106:286–92. https://doi.org/10.1016/j.applthermaleng.2016.05.144.

[12] Alsaman AS, Askalany AA, Harby K, Ahmed MS. Performance evaluation of a solar-driven adsorption desalination-cooling system. Energy 2017;128:196–207. https://doi.org/10.1016/j.energy.2017.04.010.

[13] Thu K, Yanagi H, Saha BB, Ng KC. Performance investigation on a 4-bed adsorption desalination cycle with internal heat recovery scheme. Desalination 2017;402:88–96. https://doi.org/10.1016/j.desal.2016.09.027.

[14] Youssef PG, Dakkama H, Mahmoud SM, AL-Dadah RK. Experimental investigation of adsorption water desalination/cooling system using CPO-27Ni MOF. Desalination 2017;404:192–9. https://doi.org/10.1016/j.desal.2016.11.008.

[15] Shahzad MW, Thu K, Kim Y deuk, Ng KC. An experimental investigation on MEDAD hybrid desalination cycle. Appl Energy 2015;148:273–81. https://doi.org/10.1016/j.apenergy.2015.03.062.

[16] Saha BB, El-Sharkawy II, Shahzad MW, Thu K, Ang L, Ng KC. Fundamental and application aspects of adsorption cooling and desalination. Appl Therm Eng 2016;97:68–76. https://doi.org/10.1016/j.applthermaleng.2015.09.113.

[17] Thu K, Kim YD, Shahzad MW, Saththasivam J, Ng KC. Performance investigation of an advanced multi-effect adsorption desalination (MEAD) cycle. Appl Energy 2015;159:469–77. https://doi.org/10.1016/j.apenergy.2015.09.035.

[18] Olkis C, Brandani S, Santori G. Design and experimental study of a small scale adsorption desalinator. Appl Energy 2019; 253: 113584. https://doi.org/10.1016/j.apenergy.2019.113584.

[19] Askalany AA, Freni A, Santori G. Supported ionic liquid water sorbent for high throughput desalination and drying. Desalination 2019;452:258–64. https://doi.org/10.1016/j.desal.2018.11.002.

[20] Askalany AA, Saha BB, Ismail IM. Adsorption isotherms and kinetics of HFC410A onto activated carbons. Appl Therm Eng 2014;72:237–43. https://doi.org/10.1016/j.applthermaleng.2014.04.075.

[21] Ghazy M, Askalany AA, Harby K, Ahmed MS. Adsorption isotherms and kinetics of HFC-404A onto bituminous based granular activated carbon for storage and cooling applications. Appl Therm Eng 2016;105:639–45. https://doi.org/10.1016/j.applthermaleng.2016.03.057.

[22] El-Sharkawy MM, Askalany AA, Harby K, Ahmed MS. Adsorption isotherms and kinetics of a mixture of Pentafluoroethane, 1,1,1,2-Tetrafluoroethane and Difluoromethane (HFC-407C) onto granular activated carbon. Appl Therm Eng 2016;93:988–94. https://doi.org/10.1016/j.applthermaleng.2015.10.077.

[23] Dreisbach F, Lösch H. Magnetic suspension balance for simultaneous measurement of a sample and the density of the measuring fluid. J Therm Anal Calorim 2000;62:515–21.

[24] Sircar S, Hufton JR. Why does the linear driving force model for adsorption kinetics work? Adsorption 2000;6:137–47.

[25] Saha BB, Kashiwagi T. Experimental investigation of an advanced adsorption refrigeration cycle. ASHRAE Trans 1997;103:50.

[26] Askalany AA, Salem M, Ismail IM, Ali AHH, Morsy MG. Experimental study on adsorption–desorption characteristics of granular activated carbon/R134a pair. Int J Refrig 2012;35:494–8.

[27] Askalany AA, Ernst SJ, Hügenell PPC, Bart HJ, Henninger SK, Alsaman AS. High potential of employing bentonite in adsorption cooling systems driven by low grade heat source temperatures. Energy 2017;141:782–91. https://doi.org/10.1016/j.energy.2017.07.171.

[28] Ali ES, Askalany AA, Harby K, Diab MR, Alsaman AS. Adsorption desalination-cooling system employing copper sulfate driven by low grade heat sources. Appl Therm Eng 2018;136:169–76. https://doi.org/10.1016/j.applthermaleng.2018.03.014.

[29] Ali ES, Harby K, Askalany AA, Diab MR, Alsaman AS. Weather effect on a solar powered hybrid adsorption desalination-cooling system: A case study of Egypt's climate. vol. 124. 2017. https://doi.org/10.1016/j.applthermaleng.2017.06.048.

[30] Askalany AA, Ali ES. A new approach integration of ejector within adsorption desalination cycle reaching COP higher than one. Sustain Energy Technol Assessments 2020;41:100766. https://doi.org/10.1016/j.seta.2020.100766.

[31] Cranston J, Askalany AA, Santori G. Efficient drying in washer dryers by combining sorption and heat pumping Energy 2019; 183: 683-692

[32] Talib Hussain, Laura J. Waters, Gareth M.B. Parkes, Yasser Shahzad. Microwave processed solid dispersions for enhanced dissolution ofgemfibrozil using non-ordered mesoporous silica. Colloids and Surfaces A: Physicochem. Eng. Aspects 2017; 520:428–435.